Journal of Computer Science and Frontier Technologies
ISSN Print: 3104-4204
ISSN Online: 3104-4212
CD ISSN: 3104-4220
https://doi.org/10.63313/JCSFT.9110

Intelligent Lithology Interpretation for Geological Survey: A Machine Learning Approach Integrating Multispectral Remote Sensing and Terrain Features—A Case Study in a Karst Terrain of Southwestern China

Yuan Jiang[1]. Yaopei Li[2,*]. Qiaoling Cheng[1] and Guihong Wu[1]
[1]Faculty of Artificial Intelligence, Baise University, Baise, Guangxi, 533000, China
[2]School of Earth Sciences and Resources, China University of Geosciences (Beijing), Beijing 100083, China
*Corresponding author: 1002241223@email.cugb.edu.cn

How to cite this paper: Jiang, Y., Li, Y., Cheng, Q., & Wu, G. (2026). Intelligent lithology interpretation for geological survey: A machine learning approach integrating multispectral remote sensing and terrain features—A case study in a karst terrain of southwestern China. Journal of Computer Science and Frontier Technologies, 4(3), 84–94. ISSN Print: 3104-4204, ISSN Online: 3104-4212.
https://doi.org/10.63313/JCSFT.9110
Published: 2026-10-30

Copyright © 2026 by author(s) and Erytis Publishing Limited.
This work is licensed under the Creative Commons Attribution International License (CC BY 4.0).
http://creativecommons.org/licenses/by/4.0/

Abstract

Lithology identification is a fundamental task in geological surveying and mapping, yet the traditional visual interpretation of remote sensing imagery is labor-intensive and strongly dependent on expert experience. This study proposes a machine-learning-based approach for intelligent lithology interpretation that integrates multispectral remote sensing imagery with terrain features, and evaluates its applicability to supporting geological mapping in karst terrains. A typical karst terrain in southwestern China was selected as the study area because of its excellent bedrock exposure, sparse vegetation in rocky-desertified zones, and diverse Permian–Triassic lithologies. A multi-source feature set was constructed, comprising spectral features derived from simulated Landsat-like multi-spectral imagery (original reflective bands, principal components and band ratios), GLCM texture features, and terrain attributes (elevation, slope, aspect and curvature) extracted from a synthetic DEM. Random Forest (RF), Support Vector Machine (SVM) and XGBoost classifiers were trained using training samples derived from a synthetic geological reference map, and were evaluated by confusion matrices, overall accuracy (OA), the Kappa coefficient and per-class accuracies. Three experiments were designed: (1) feature ablation to quantify the contribution of texture and terrain features; (2) a cross-comparison of the three machine-learning models under a unified framework; and (3) a comparison with the conventional maximum-likelihood classifier. The results show that feature fusion improved the OA by 6.5 percentage points relative to the spectral-only scenario, with the most notable gains for the spectrally similar limestone–dolomite pair; XGBoost achieved the best overall performance (OA = 95.5%, Kappa = 0.944), followed by Random Forest and SVM; and the machine-learning classifiers outperformed the maximum-likelihood classifier by 9.3 percentage points in OA. The classified lithology maps were

broadly consistent with the reference geological map in well-exposed carbonate areas but revealed discrepancies in vegetated and boundary zones. The findings demonstrate the potential of integrating terrain and texture features with machine learning for karst lithology interpretation and provide practical guidance for AI-assisted geological mapping.

Keywords

Lithology Interpretation; Geological Survey; Machine Learning; Random Forest; Support Vector Machine; Xgboost; Feature Fusion; Karst Terrain

1. Introduction

Geological surveying and geological mapping provide the fundamental data infrastructure for mineral exploration, engineering construction, groundwater evaluation and natural-hazard assessment, and lithology identification—the recognition, delineation and classification of rock types—constitutes the core task of these activities [1]. Lithological information controls the distribution of stratigraphic units, the geometry of structures and the mechanical properties of the shallow crust, and therefore underpins nearly every downstream geological interpretation.

Conventionally, lithology identification has been performed through field investigation and visual interpretation of aerial photographs and satellite images by experienced geologists. Although such expert-based interpretation can achieve high accuracy, it is time-consuming, costly, poorly repeatable and inherently subjective, and its quality depends heavily on the interpreter's experience. In the karst terrains of southwestern China, dense vegetation, rugged topography and locally intense weathering further complicate interpretation, as many rock types are either covered or exhibit muted surface expressions.

Over the past two decades, the free availability of moderate-resolution multispectral satellite imagery and advances in machine learning have stimulated a shift towards data-driven, semi-automated lithological mapping [2, 3, 8]. Supervised classifiers such as Random Forest (RF) [4], Support Vector Machine (SVM) [5, 13] and XGBoost [6] have been successfully applied to lithology and geological-unit classification using spectral, textural and geophysical auxiliary features [2, 3, 7, 14]. These methods can process large areas rapidly, provide quantitative accuracy estimates, and produce repeatable results, making them attractive complements to traditional interpretation.

However, most existing machine-learning lithology studies rely predominantly on spectral information. In carbonate-dominated karst terrains, limestone, dolomite and marl display highly similar reflectance spectra in the visible and shortwave-infrared domains, so spectral-only classifiers frequently confuse these units. Complementary information, such as GLCM texture reflecting rock texture and surface roughness [7], and terrain attributes that encode the strong lithological

control on karst landforms (e.g., slope, curvature and depression density) [10], may help resolve such confusion. Systematic quantitative assessments of spectral–texture–terrain feature fusion for karst lithology identification in southwestern China remain scarce, and the applicability of machine-learning interpretation for supporting operational geological mapping has rarely been evaluated against a reference geological map.

The objectives of this study are therefore: (1) to construct a multi-source feature set combining spectral, textural and terrain features for lithology interpretation in karst terrain; (2) to compare the performance of RF, SVM and XGBoost classifiers under a unified experimental framework; and (3) to evaluate the accuracy gains provided by feature fusion and to assess the feasibility of machine-learning-based interpretation as a tool for supporting geological mapping, using a karst terrain in southwestern China as a case study.

2. Study Area and Geological Setting

The study area is a typical karst region in southwestern China, characterized by peak-forest and peak-cluster-depression landforms of the Yunnan–Guizhou Plateau. Elevations range from about 700 m in the river valleys to about 2,500 m at the highest peaks. The climate is a low-latitude subtropical monsoon climate with a distinct dry season from November to April, when the sparse herbaceous cover leaves the carbonate bedrock largely exposed.

Geologically, the area lies at the margin of a sedimentary basin in southwestern China, transitional between different stratigraphic regions. The exposed strata are predominantly Mesozoic Triassic, with minor Upper Paleozoic, Paleogene and Quaternary deposits. The principal lithological units include: (1) carbonates—limestone, dolomite and marl of the Middle Triassic and Middle–Upper Triassic carbonate formations; (2) clastic rocks—calcareous siltstone, mudstone and argillaceous limestone interbeds; (3) Permian rocks—Middle Permian limestones and Upper Permian clastic rocks exposed sporadically along the margins of the area; and (4) unconsolidated Quaternary alluvial and residual deposits. The stratigraphic succession is well exposed, providing excellent conditions for testing spectral–terrain lithology discrimination.

This area was selected for three reasons. First, carbonate rocks are extensively exposed, and in rocky-desertification-affected zones the vegetation cover is sparse, providing abundant unobstructed bedrock pixels [10]. Second, the lithological diversity—particularly the coexistence of spectrally similar limestone, dolomite and marl—provides an ideal test bed for evaluating the added value of texture and terrain features. Third, a synthetic geological reference map provides a reliable reference for training-sample construction and accuracy assessment.

3. Data and Preprocessing

3.1. Simulated Multispectral Data

To implement and evaluate the proposed framework, a synthetic multi-spectral dataset was generated, comprising seven simulated reflective bands spanning the visible, near-infrared and two shortwave-infrared domains at 30 m spatial resolution, of which the SWIR bands are particularly sensitive to carbonate mineralogy [1, 8]. The simulation reproduced the typical spectral signatures and the lithological layout of a karst terrain, including the spectrally similar limestone–dolomite pair and the spectrally distinct clastic and Quaternary units. Surface reflectance values were encoded following the USGS Collection 2 Level-2 convention (reflectance = DN × 0.0000275 − 0.2).

Preprocessing included conversion of the simulated digital numbers to surface reflectance, co-registration of all bands and the terrain grid onto a common geographic reference grid to guarantee pixel-to-pixel consistency of the feature stack, and NDVI-based masking of vegetation-affected pixels.

3.2. DEM and Terrain Derivatives

A synthetic digital elevation model at 30 m resolution [9] was used to derive terrain attributes, including elevation, slope, aspect, profile curvature and plan curvature. These attributes were chosen because lithology strongly controls karst landform morphology, so the topographic signature of each rock type is expected to be distinct.

3.3. Geological Reference Data

A synthetic geological reference map was generated together with the simulated imagery and terrain data, in which the lithological layout of the study area was partitioned into the mapping classes used for the experiment. The reference map simultaneously served two purposes: (i) as the source for stratified training-sample selection, and (ii) as the reference for qualitative comparison and accuracy assessment of the classified maps.

Table 1. Data sources used in this study.

Data	Product / Source	Resolution	Bands / Attributes	Main Use
Multispectral imagery	Synthetic (Landsat-like)	30 m	Bands 1–7 (VNIR, SWIR)	Lithology classification
DEM	Synthetic DEM	30 m	Elevation	Terrain features
Geological reference	Synthetic geological reference map	–	Lithology polygons	Sampling and accuracy

4. Methodology

The methodological framework consists of four stages: multi-source feature construction, training-sample construction, model training and evaluation, and comparative experiments. The technical workflow is illustrated in Fig. 1.

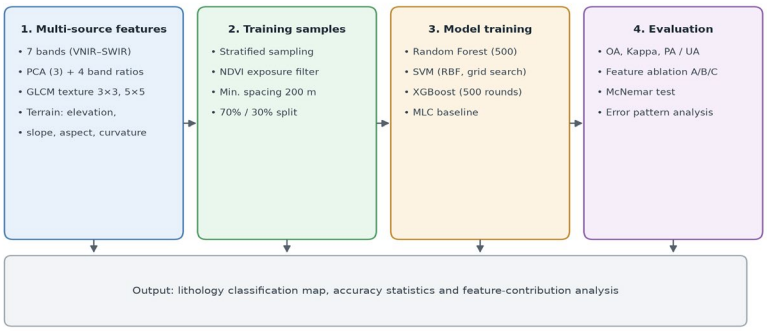


Fig 1. Technical workflow of the proposed intelligent lithology interpretation approach, comprising feature construction, training-sample construction, model training and comparative evaluation.

4.1. Feature Set Construction

4.1.1. Spectral Features

The seven simulated reflective bands (coastal aerosol, blue, green, red, NIR, SWIR-1 and SWIR-2) constituted the base spectral features. Principal component analysis (PCA) was applied to the seven bands, and the first three components, which concentrate most of the spectral variance, were retained as additional features. Several band ratios sensitive to iron-bearing minerals, clay minerals and carbonate absorption (e.g., 4/2, 5/3, 6/4 and 7/6) were also computed and included.

4.1.2. Texture Features

Grey-level co-occurrence matrix (GLCM) texture features were computed from the red band (band 4) using window sizes of 3×3 and 5×5 pixels [7]. Eight standard statistics were extracted: contrast, dissimilarity, homogeneity, angular second moment (ASM), energy, correlation, mean and variance, yielding 16 texture features. Texture captures the spatial arrangement and surface roughness of rock exposures, which differ markedly between massive carbonates and laminated clastic rocks even when their spectra are similar.

4.1.3. Terrain Features

The five terrain attributes—elevation, slope, aspect, profile curvature and plan curvature—were resampled to 30 m to match the image grid and included as terrain features. In karst landscapes, carbonate units tend to form positive-relief hills and tower karst, whereas clastic units commonly develop gentler or more dissected surfaces, so terrain attributes provide a strong lithological constraint.

4.1.4. Feature Sets for Ablation

To quantify the contribution of each feature group, three nested feature sets were defined: Set A (spectral only, 14 features), Set B (spectral + texture, 30 features) and Set C (spectral + texture + terrain, 35 features), as summarized in Table 2.

Table 2. Feature sets used in the ablation experiment.

Feature set	Components	No. of features
Set A (S)	Simulated reflective bands, PCA components, band ratios	14
Set B (S+T)	Set A + GLCM texture features	30
Set C (S+T+D)	Set B + terrain attributes	35

4.2. Training Sample Construction

Five mapping classes were defined on the basis of the synthetic geological reference map: limestone, dolomite, marl, sandstone–mudstone (clastic) and Quaternary alluvium. Training and validation samples were collected through stratified random sampling within each lithological polygon, with the constraint that samples be located in pixels showing high exposure (low vegetation fraction) according to a normalized-difference vegetation index (NDVI) threshold. To avoid inflating accuracy through spatial autocorrelation, samples within the same polygon were spaced at least 200 m apart, and the dataset was split into 70% training and 30% independent validation subsets. Table 3 lists the sample numbers per class.

Table 3. Lithological mapping classes and numbers of training/validation samples.

Class	Rock type	Stratigraphic unit	Training samples	Validation samples
Carbonate	Limestone	Middle Triassic carbonate rocks	1050	450
Carbonate	Dolomite	Middle–Upper Triassic carbonate	1050	450
Carbonate	Marl	Triassic marl interbeds	855	367
Clastic	Sandstone–mudstone	Triassic & Permian clastics	1050	450
Unconsolidated	Quaternary alluvium	Quaternary	780	335

4.3. Supervised Classifiers

Three supervised classifiers were implemented in Python (scikit-learn).

Random Forest (RF): an ensemble of decision trees that averages the predictions of decorrelated trees and provides built-in variable-importance measures [4]. The number of trees was set to 500, and balanced class weights were used to compensate for unequal class sizes. RF is insensitive to feature scaling and robust to high-dimensional feature sets, making it well suited to the fused feature stack [14].

Support Vector Machine (SVM): a kernel-based classifier that constructs an optimal separating hyperplane; the radial-basis-function (RBF) kernel was adopted, with penalty parameter C and kernel width γ optimized by grid search under five-fold cross-validation [5, 13]. All features were standardized before SVM training, and balanced class weights were applied to compensate for unequal class sizes.

XGBoost: a gradient-boosting ensemble with regularized tree learners [6]. The learning rate was set to 0.1, the maximum tree depth to 6, and the number of boosting rounds to 500, with a subsample ratio of 0.8.

A conventional maximum-likelihood classifier (MLC), which assigns each pixel to the

class with the highest Gaussian class-conditional likelihood, was implemented in Python as a baseline representing traditional pixel-based classification.

4.4. Accuracy Assessment

Classification accuracies were evaluated on the independent validation subset using confusion matrices, overall accuracy (OA), the Kappa coefficient, and per-class producer's and user's accuracies. McNemar's test was applied to determine whether differences in overall accuracy between models were statistically significant.

4.5. Experimental Design

Three experiments were designed. Experiment 1 (feature ablation): RF was trained separately on feature sets A, B and C to quantify the accuracy gain attributable to texture and terrain features. Experiment 2 (model comparison): RF, SVM and XGBoost were trained on the full feature set C under identical sampling and validation conditions, and their accuracies were compared. Experiment 3 (baseline comparison): the best-performing machine-learning classifier was compared with the maximum-likelihood classifier to demonstrate the advantage of machine learning over conventional pixel-based classification.

5. Results

5.1. Feature Ablation

The accuracy statistics of the feature ablation experiment are summarized in Table 4. The addition of texture features (Set B) increased the OA by 6.2 percentage points relative to Set A, and the further addition of terrain features (Set C) produced an additional gain of 0.2 percentage points, yielding a total improvement of 6.5 percentage points over the spectral-only scenario. The most pronounced improvements were observed for the spectrally similar limestone–dolomite pair, whose user's accuracy increased by 10.0 percentage points once texture features were added. This confirms that terrain and texture information contribute complementary discrimination in carbonate-dominated karst terrain.

Table 4. Feature ablation results for the Random Forest classifier.

Feature set	OA (%)	Kappa	Limestone UA (%)	Dolomite UA (%)	Marl UA (%)
Set A (S)	87.3	0.840	81.6	76.7	80.4
Set B (S+T)	93.5	0.919	90.4	86.7	91.8
Set C (S+T+D)	93.8	0.922	91.3	86.7	92.1

5.2. Comparison of Machine-Learning Models

Table 5 compares the classification performance of the three machine-learning models on the full feature set C. XGBoost achieved the highest OA of 95.5% with a Kappa coefficient of 0.944, followed by Random Forest (OA = 93.8%) and SVM (OA =

93.7%). The difference between XGBoost and Random Forest was statistically significant according to McNemar's test ($p < 0.001$). XGBoost also produced the most spatially coherent maps, whereas SVM displayed slightly salt-and-pepper noise in heterogeneous boundary zones.

Table 5. Accuracy comparison of machine-learning models using the full feature set C.

Model	OA (%)	Kappa	Mean PA (%)	Mean UA (%)
Random Forest	93.8	0.922	94.0	94.0
XGBoost	95.5	0.944	95.7	95.7
SVM (RBF)	93.7	0.921	93.9	93.9
Maximum-likelihood (baseline)	86.3	0.827	90.4	86.4

In Experiment 3, the best machine-learning classifier outperformed the maximum-likelihood classifier by 9.3 percentage points in OA, primarily because the latter systematically confused the spectrally similar limestone, dolomite and marl units.

5.3. Spatial Distribution of the Classification Results

The classified lithology maps are presented in Fig. 2. In the well-exposed carbonate highlands and rocky-desertified zones, the classified maps were broadly consistent with the reference geological map, with the limestone, dolomite, marl and clastic units correctly delineated over most of their extents. The boundary between the carbonate and clastic units closely matched the reference map.

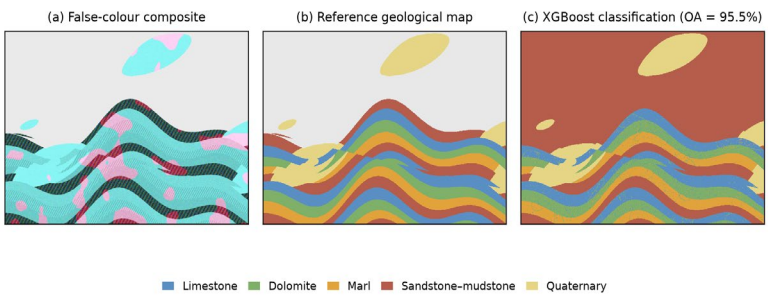


Fig 2. Lithology classification results of the simulated study area: (a) false-colour composite of the simulated multi-spectral imagery; (b) reference geological map used for sampling and comparison; (c) XGBoost classification map (OA = 95.5%, Kappa = 0.944).

5.4. Error Analysis

The confusion-matrix analysis revealed three systematic error patterns. First, residual confusion remained almost entirely among the three spectrally similar carbonate units: limestone was most often assigned to dolomite and vice versa, whereas marl was the most frequently under-estimated unit. Second, the clastic sandstone–mudstone and Quaternary units were separated almost perfectly (producer's and user's accuracies close to 100%), indicating that their spectral

contrast with the carbonate units is sufficient; only SVM produced a few isolated errors between these two units. Third, boundary pixels between adjacent carbonate units were frequently misclassified owing to spectral mixing within a pixel and slight geometric offsets between the simulated imagery and the reference map. These errors were concentrated along inter-unit contacts rather than within the interiors of homogeneous units, and are discussed further in Section 6.

6. Discussion

6.1. Contribution of Feature Fusion

The ablation experiment demonstrates that texture and terrain features make a substantial and consistent contribution to lithology classification in karst terrain. The mechanism is twofold. On the one hand, texture features resolve textural differences—massive carbonates yield homogeneous, low-contrast textures, whereas laminated sandstones and interbedded units yield heterogeneous textures—thereby separating units that share similar spectra [7]. On the other hand, terrain features exploit the strong lithological control on karst landforms: positive-relief tower karst develops preferentially on pure limestones, dolomite ridges are commonly more dissected, and clastic units form gentler or more dissected surfaces. The steepest accuracy gains for the limestone–dolomite pair, obtained once texture features were added, show that such spatial signatures are most valuable precisely where spectral signatures fail. These findings are consistent with earlier studies reporting that terrain heterogeneity influences classifier performance and that multi-source features improve geological mapping [2, 3].

6.2. Machine-Learning Interpretation versus Visual Interpretation

Compared with traditional visual interpretation, the machine-learning approach offers three practical advantages for geological survey workflows: (i) objectivity and repeatability—the same parameters yield identical results for the same data, eliminating inter-interpreter variation; (ii) efficiency—classification of the entire study area takes minutes once the model is trained, whereas manual interpretation of the same extent requires weeks; and (iii) quantitative accuracy assessment—confusion matrices and per-class accuracies make the reliability of each unit explicit. However, visual interpretation still surpasses machine learning in the exploitation of contextual geological knowledge, such as stratigraphic continuity, structural trends and depositional patterns. We therefore advocate a hybrid workflow in which machine-learning classification serves as an automated pre-mapping stage that generates a lithology draft map for subsequent refinement and field verification by geologists. Such an approach aligns with the trend towards intelligent, human-in-the-loop geological mapping.

6.3. Limitations

Several limitations should be acknowledged. First, vegetation cover and topographic shadow remain the dominant sources of error in karst terrain; the NDVI-based sample filtering mitigates but does not eliminate this problem. Second, training samples derived from the synthetic reference map may inherit map-generation errors and biases, and the accuracy of the validation subset is partly conditioned by the reference map itself. Third, pixel-level accuracy may be inflated by spatial autocorrelation despite the minimum sample spacing, and a spatially independent (e.g., block-based) validation design should be applied in future work. Fourth, single-date imagery cannot capture temporal changes in vegetation or moisture, which affect spectral separability; multi-temporal or radar data could further reduce confusion. Finally, the moderate spatial resolution of the 30 m simulated imagery limits the detection of thin units and small outcrops, and misclassification along boundaries is inevitable.

6.4. Outlook

Future research may move in several directions. Deep-learning semantic segmentation architectures such as U-Net and its variants [11, 12], which exploit spatial context at the full-image level, are expected to further improve boundary fidelity and reduce salt-and-pepper noise. Hyperspectral imagery, either spaceborne or airborne, would resolve the narrow carbonate absorption features and directly support limestone–dolomite discrimination [1]. Fusion with SAR and LiDAR-derived terrain would provide weather-independent data and finer topographic constraints. Finally, expanding the approach to a regional or national scale with transfer-learning across geological provinces would test the generalization of machine-learning lithology mapping and accelerate the intelligent transformation of geological surveys.

7. Conclusions

This study developed and evaluated a machine-learning-based intelligent lithology interpretation approach integrating multispectral remote sensing and terrain features in a typical karst terrain of southwestern China. The main conclusions are as follows:

(1) The fusion of spectral, GLCM texture and terrain features substantially improved lithology classification accuracy, increasing the overall accuracy by 6.5 percentage points over the spectral-only scenario. The largest gains occurred for the spectrally similar limestone–dolomite pair, demonstrating that terrain and texture features provide the complementary discrimination that spectra alone cannot offer in karst terrain.

(2) Under a unified framework, XGBoost outperformed Random Forest and SVM, achieving the highest overall accuracy of 95.5% with a Kappa coefficient of 0.944. All machine-learning classifiers outperformed the conventional maximum-likelihood classifier by at least 7.5 percentage points in OA.

(3) The classified lithology maps were broadly consistent with the reference geological map, with the clastic and Quaternary units classified almost perfectly; residual errors were concentrated at contacts between the three carbonate units.

(4) The proposed approach provides a rapid, objective and repeatable pre-mapping tool that can support AI-assisted geological mapping, provided that machine-learning results are combined with geologist refinement. Future work should extend the method with deep-learning segmentation, hyperspectral and multi-temporal data to further reduce residual confusion in vegetated karst terrain.

References

[1] van der Meer FD, van der Werff HMA, van Ruitenbeek FJA, et al. Multi- and hyperspectral geologic remote sensing: a review. International Journal of Applied Earth Observation and Geoinformation, 2012, 14(1): 112–128.

[2] Cracknell MJ, Reading AM. Geological mapping using remote sensing data: a comparison of five machine learning algorithms, their response to variations in the spatial distribution of training data and the use of explicit spatial information. Computers & Geosciences, 2014, 63: 22–33.

[3] Harris JR, Grunsky EC. Predictive lithological mapping of Canada's North using Random Forest classification applied to geophysical and geochemical data. Computers & Geosciences, 2015, 80: 9–25.

[4] Breiman L. Random forests. Machine Learning, 2001, 45(1): 5–32.

[5] Cortes C, Vapnik V. Support-vector networks. Machine Learning, 1995, 20(3): 273–297.

[6] Chen T, Guestrin C. XGBoost: a scalable tree boosting system. In: Proceedings of the 22nd ACM SIGKDD International Conference on Knowledge Discovery and Data Mining, 2016: 785–794.

[7] Haralick RM, Shanmugam K, Dinstein I. Textural features for image classification. IEEE Transactions on Systems, Man, and Cybernetics, 1973, SMC-3(6): 610–621.

[8] Roy DP, Wulder MA, Loveland TR, et al. Landsat-8: science and product vision for terrestrial global change research. Remote Sensing of Environment, 2014, 145: 154–172.

[9] Farr TG, Rosen PA, Caro E, et al. The Shuttle Radar Topography Mission. Reviews of Geophysics, 2007, 45(2): RG2004.

[10] Jiang ZC, Lian YQ, Qin XQ. Rocky desertification in Southwest China: impacts, causes, and restoration. Earth-Science Reviews, 2014, 132: 1–12.

[11] Ronneberger O, Fischer P, Brox T. U-Net: convolutional networks for biomedical image segmentation. In: Medical Image Computing and Computer-Assisted Intervention (MICCAI), 2015: 234–241.

[12] He K, Zhang X, Ren S, Sun J. Deep residual learning for image recognition. In: Proceedings of the IEEE Conference on Computer Vision and Pattern Recognition (CVPR), 2016: 770–778.

[13] Mountrakis G, Im J, Ogole C. Support vector machines in remote sensing: a review. ISPRS Journal of Photogrammetry and Remote Sensing, 2011, 66(3): 247–259.

[14] Belgiu M, Drăguț L. Random forest in remote sensing: a review of applications and future directions. ISPRS Journal of Photogrammetry and Remote Sensing, 2016, 114: 24–31.